Enhanced Scanning Range Design for Leaky-Wave Antenna (LWA) at 60 GHz

Zhang Qiang, Julien Sarrazin, Massimiliano Casaletti, Guido Valerio, Philippe de Doncker, Aziz Benlarbi-Delai

Enhanced Scanning Range Design for Leaky-Wave Antenna (LWA) at 60 GHz

Qiang Zhang[1,2], Julien Sarrazin[1], Massimiliano Casaletti[1], Guido Valerio[1], Philippe De Doncker[2], Aziz Benlarbi-Delaï[1]

[1] Sorbonne Université, Laboratoire d'Electronique et Electromagnétisme, L2E, F-75005 Paris, France, qiang.zhang@upmc.fr

[2] Université Libre de Bruxelles (ULB), Av. Roosevelt 50, 1050 Brussels, Belgium

***Abstract*—The benefits of metasurface-based Leaky-Wave Antennas (LWA) over more conventional LWA is assessed in terms of angular scanning. In order to achieve a fast-angular scanning with frequency, a highly-dispersive waveguide is classically required. The additional degree of freedom offered by a surface impedance, here implemented with a grid of square patches enables increasing the dispersion. Using this enhanced dispersion, a LWA is designed and simulated in the 60 GHz band. It is shown that the obtained scanning range is increased by a 2.6 factor with respect to a classical LWA composed of metallic strips over a grounded dielectric Slab. A scanning range from -52° to -16° has been thus obtained with a 11.6% frequency bandwidth.**

***Index Terms*—leaky wave antenna (LWA), metasurface, transverse resonance method, dispersion analysis, wide range scanning antenna.**

I. INTRODUCTION

Periodic Leaky-Wave Antennas (LWA) have attracted a lot of attention from researchers in the past decade due to their interesting characteristics [1]. A key feature is their ability to achieve high gain using planar structures [2]. In classical LWA, the direction of the main beam radiation depends on the operating frequency. While this can be considered as a drawback in wireless communications, other applications take benefit of this specific behavior. Indeed, angular scanning capability can be used for instance for detecting vehicle collisions in Vehicle-to-Everything (V2X) communications [3], in radar applications [4], or for direction of arrival estimation for future 5G mobile telecommunication [5][6]. Recently in the e-health field, non-contact remote monitoring of human activities and vital signs (e.g., breathing and heartbeat rates) have been investigated at millimeter wave frequencies in indoor environments [7][8] and would also require scanning capabilities in order to track a person moving in room.

While solutions exist to get rid of the LWA stop-band [9] [10] which can be a problem when scanning through broadside, a fast scanning is often desired in order to cover a large angular range with a given operation frequency bandwidth. For LWA to achieve large scanning-range/bandwidth ratio, a highly dispersive structure is needed. To improve the dispersion of the classical waveguides in printed technology, different strategies can be considered such as using high permittivity substrates as mentioned in [11] or by acting on the substrate thickness. However, available low-loss planar substrates are limited in terms of dielectric constant values and increasing the substrate thickness generates higher order modes of propagation that are difficult to deal with. Other approaches can be implemented in order to increase the scanning range such as the one in [12], where a high scanning sensitivity LWA is theoretically presented using Gain-Loss C-Section Phasers. Nonetheless, the antenna is difficult to be realized and consumes a large amount of power for high sensitivity solution.

Another method is to artificially make the substrate denser by using metasurfaces. It is therefore possible to change the electromagnetic behavior of a waveguide in order to increase to some extent its frequency dispersion. In [13], a periodic LWA using sinusoidally modulated surface impedance composed of a grid of strips on a Grounded Dielectric Slab (GDS) is investigated but the scanning capability is not deeply discussed.

In this paper, to provide an enhanced scanning range LWA with simple fabrication, the Transvers Resonance Method (TRM) is firstly applied to investigate analytically the dispersion of different structures (GDS and GDS covered with metasurface) in section II. The enhanced LWA design procedure is then described in section III. In section IV, the performances of the LWA with and without metasurface are compared and full-wave simulation results are shown. Lastly, conclusion and perspective are given in section V.

II. DISPERSION ANALYSIS

A. Grounded Dielectric Slab (GDS)

A GDS is a classic surface wave guide that supports only TM and TE propagation modes. Fig. 1 shows the cross-sectional geometry of the GDS in xz-plane, which is composed of 2 layers: the air and the grounded dielectric. The dimensions along y-axis and z-axis of the GDS are assumed to be infinite, in order to simplify the dispersion calculation, so that the confined waves reflect only in the transverse direction (along the x-axis). The intrinsic wavenumber of each layer is given by $k_i = \omega\sqrt{\varepsilon_i \mu_i}$, where ω, ε_i and μ_i represent the angular frequency, the permittivity and the permeability of the layer "i" respectively. The wave vector in each layer k_i is decomposed into two components: k_t in the transverse direction (x-axis) and β in the direction of propagation (z-axis) as:

$$k_i^2 = k_t^2 + \beta^2 \quad (1)$$

Neglecting the losses within the waveguide, the convention $e^{-j\beta z}$ is used to describe positive z-axis wave propagation.

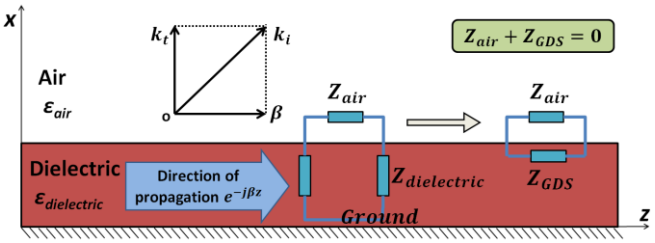

Fig. 1. Transverse resonance method for grounded dielectric slab

To satisfy the propagation condition, β in each layer should be identical. And for propagation modes to exist, k_t should satisfy the TRM condition:

$$Z_{air}^{TE/TM} + Z_{GDS}^{TE/TM} = 0 \quad (2)$$

where $Z_{air}^{TE/TM}$ and $Z_{GDS}^{TE/TM}$ are the input impedances seen looking to the upside and downside respectively at the air-dielectric surface [14]. $Z_{GDS}^{TE/TM}$ is the grounded slab impedance seen at the air-dielectric surface:

$$Z_{GDS}^{TE/TM} = jZ_{dielectric}^{TE/TM} \tan(k_{t\_dielectric} l) \quad (3)$$

where l is the thickness of substrate and $k_{t\_dielectric}$ the transverse wave vector component of the dielectric layer.

The transverse impedance of a homogenous layer, i.e., $Z_{air}^{TE/TM}$ and $Z_{dielectric}^{TE/TM}$, are given for the TM mode (magnetic field normal to the x-z plane) by

$$Z_i^{TM} = \frac{k_t}{\omega \varepsilon_i} \quad (4)$$

and TE mode (electric field normal to the x-z plane) by

$$Z_i^{TE} = \frac{\omega \mu_i}{k_t} \quad (5)$$

Using this method, solutions of β were found numerically in Matlab and verified by full-wave simulations using CST Microwave Studio.

B. GDS covered with Metasurface (GDSM)

For the GDS covered with a metasurface, the calculation is similar to the previous one except that the metasurface transverse impedance $Z_{patch}^{TE/TM}$ is inserted in parallel with the $Z_{GDSM}^{TE/TM}$ (see Fig. 2) into the TRM equation. The dispersion equation therefore becomes:

$$Z_{air} + Z_{GDSM} // Z_{patch} = 0 \quad (6)$$

The metasurface used in this paper is a lattice of square patches, whose transverse impedance can be analytically

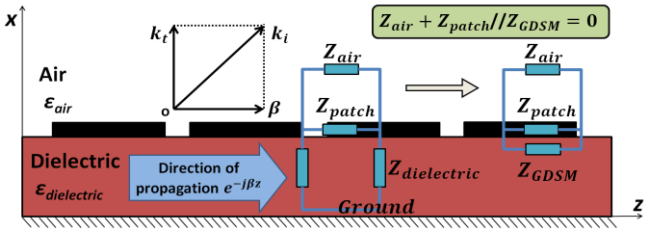

Fig. 2. Transverse resonance method for grounded dielectric slab covered with metasurface

related to the physical dimensions using expression given in [15] for both TM and TE modes. The solutions for β can then be solved using the same numerical method for the classical GDS. It should be noticed that the transverse impedance $Z_{GDSM}^{TE/TM}$ is naturally different from the $Z_{GDS}^{TE/TM}$ since the electromagnetic behavior of the guide is modified by the addition of the metasurface as shown in the next section.

III. Enhanced Dispersive GDS with Patches Grid Metasurface

In order to increase the scanning range of a LWA, we propose to increase the dispersion of the waveguide that support the surface-wave propagation. To do so, a possibility is to use denser materials. This can be achieved by using high permittivity materials but large values are not easily available as planar low loss substrates. Another possibility is to use metasurface to artificially make denser the GDS. To assess these two solutions with respect to classical GDS, we define three waveguides of identical thickness:

1. GDSL – the original low dispersive GDS whose permittivity of substrate is ε_l,
2. GDSH – the objective high dispersive GDS whose permittivity of substrate is $\varepsilon_h > \varepsilon_l$,
3. GDSM – the enhanced GDSL that includes a metasurface.

The goal is to design a GDSM that mimics the dispersive behavior of the GDSH while using the same low permittivity substrate as the GDSL. To do so, the GDSH dispersion is firstly studied with the model in Fig. 1. Only TM_0 mode is here considered as it is the one that will become leaky in the next section. However, it has been verified that no higher order modes exist within the frequency range of interest. $Z_{GDSH}^{TM} = jX$ and β_{GDSH} at a given frequency f_0 are determined. Z_{patch} is then calculated in order to satisfy the following condition:

$$Z_{GDSM}^{TM} // Z_{patch}^{TM} = jX \quad (7)$$

where

$$Z_{GDSM}^{TM} = j\frac{\sqrt{\omega_0^2 \varepsilon_0 \varepsilon_l \mu_0 - \beta_{GDSH}^2}}{\omega_0 \varepsilon_l} tan\left(\sqrt{\omega_0^2 \varepsilon_0 \varepsilon_l \mu_0 - \beta_{GDSH}^2} l\right) \quad (8)$$

and Z_{patch}^{TM} is a pure reactance as shown in [15] (for loss-less electric conductors).

The design is performed at f_0 = 60 GHz and Fig. 3 shows the dispersion diagram in the license-free 57-64 GHz band for the three considered structures. The GDSL uses a Rogers RT6010 substrate with ε_l = 10.2, the GDSH considers a substrate with ε_h = 20, and the GDSM mimics the GDSH at f_0 using the RT6010 substrate and $Z_{patch}^{TM} = \frac{1}{jC\omega_0}$ (with C = 11.9 fF, considered constant over the frequency range). The thickness of the substrate is 0.254 mm for all three structures and is chosen such that only the fundamental TM_0 mode propagates in the operation band.

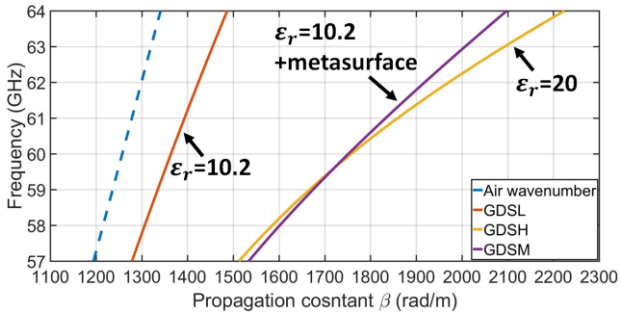

Fig. 3. Dispersion curves for GDSL, GDSH and GDSM

The propagation constant varies from 1280 to 1485 rad/m for the GDSL (about 29 rad/m/GHz under linear approximation) and from 1516 to 2217 rad/m for the GDSH (about 100 rad/m/GHz under linear approximation). As expected, the dispersion has increased by changing the permittivity of substrate from 10.2 to 20. The dispersion of designed GDSM is similar to the GDSH and varies from 1537 to 2094 rad/m (about 80 rad/m/GHz under linear approximation). So, using the same RT6010 substrate, the GDSM is about 2.76 times more dispersive than the GDSL.

The geometrical dimensions of the square patches that compose the metasurface can be calculated analytically using the relations in [15]:

$$C = \frac{2\varepsilon_0\varepsilon_{eff}D\ln\left(\frac{1}{\sin\frac{\pi W}{2D}}\right)}{\pi} \quad (9)$$

where D is the spatial periodicity of the metasurface lattice, W is the gap width between two adjacent patches and ε_{eff} is the effective permittivity calculated as $\varepsilon_{eff} = \frac{\varepsilon_l+1}{2}$. The gap width is firstly fixed at W = 0.05 mm. The spatial periodicity D is then calculated using eq. (9) as D = 0.287 mm which represents $\lambda_0/17.4$ or $\lambda_g/12.5$ where λ_0 and λ_g are the free-space and guided wavelengths respectively at 60 GHz. The patch size is therefore 0.237 mm. Although there are unlimited choices for the metasurface design, the above dimensions have been chosen as a tradeoff between achieving small lattice periodicity to meet the homogenization assumptions made in [15] and the considered fabrication process accuracy (i.e., 50 µm minimum gap size with laser etching). Also, it is convenient to choose D as an integer fraction of the periodicity p of the LWA as seen in the next section.

IV. Leaky-wave Antenna Design

With the GDSM structure presented in section III, a periodic LWA is designed by deleting periodically a line of patches along the direction of propagation of a surface TM_0 wave. The addition of this periodicity creates an infinite number of space harmonics [16], and the propagation constant of the n-nth harmonic can be calculated as:

$$\beta_n = \beta + \frac{n2\pi}{p} \quad (10)$$

where β is the propagation constant of the GDSM, p is the spatial period of LWA (i.e., the distance between deleted periodic lines), and n an integer value from the negative infinity to positive infinity. If the n-nth harmonic enters into the fast wave zone, i.e., $-k_0 < \beta_n < k_0$, where k_0 is the air wavenumber, the surface wave will leak into the air in the following direction with respect to broadside:

$$\theta = \sin^{-1}(\beta_n/k_0) \quad (11)$$

We define the period p of the LWA as $p = mD$, and m is a positive integer value. This period is chosen as 2.583 mm in this paper (i.e., m = 9) in order to radiate the harmonic β_{-1} in the backward direction at θ = -14° at f = 64 GHz and keep the others harmonics confined in the guide (in the slow wave zone).

Fig. 4a and Fig. 4b show the classical strip LWA design and the GDSM-based design respectively. The periodicity of the classical LWA is chosen such to radiate at f = 64 GHz toward to the same direction than the GDSM-based LWA, that is p = 3.5 mm. The metallic strips are 0.8 mm wide along the z-axis. Both antennas have 15 periods p and the total length of the classic LWA and the designed LWA are 55 mm and 39 mm respectively. The antenna widths are identical and equal to 10 mm. These two antennas are simulated with CST Microwave Studio using a waveguide port excitation at both ends. The substrate relative permittivity is ε_r = 10.2 and $\tan\delta$ = 0.0023, and the ohmic

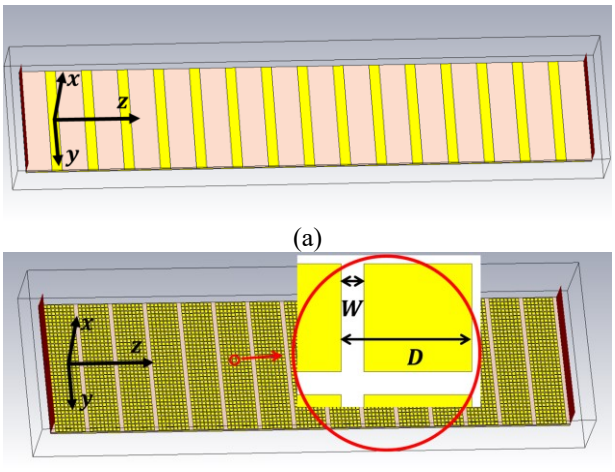

(a)

(b)

Fig. 4. LWA design: classical metallic strip LWA (a) and GDSM-based LWA (b)

losses in the metal (including the ground plane) are defined using a conductivity $\sigma = 5.8\times10^7$ S/m.

Fig. 5a and 5b show the simulated radiation pattern along the x-z plane of the classical LWA and the GDSM-based LWA respectively. The scanning range over the 57-64 GHz bandwidth of the classical LWA spans from -28° to -14° while the metasurface scans from -52° to -16°. So, an improvement of a 2.6 ratio is achieved as expected from the dispersion analysis. Furthermore, using equation (11), the scanning range of the GDSM-based LWA is theoretically calculated to be -49° to -14° while the classical LWA spans from -26° to -13°, which is in good agreement with the full-wave simulations.

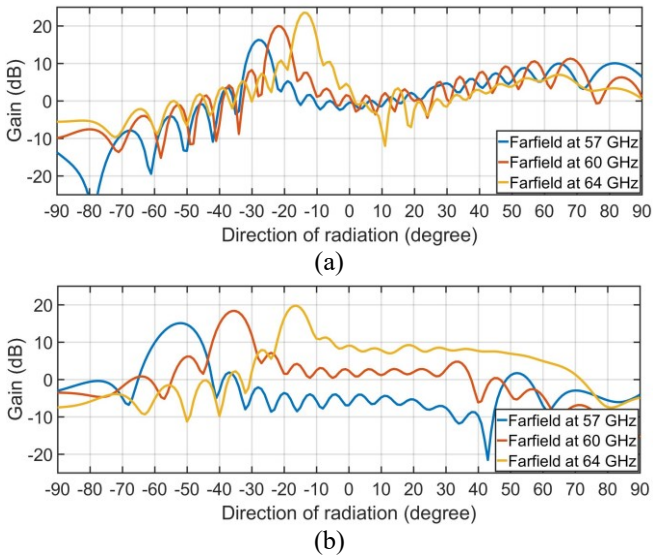

Fig. 5. Radiation pattern in x-z plane of the classical LWA and the GDSM-based LWA

As no specific care has been devoted to the attenuation constant of the leaky-wave, a variation of maximum gain with respect to the frequency is observed. However, this variation is slightly smaller with the GDSM-based LWA (27% over the 7 GHz bandwidth) than with the classical design (36% over the 7 GHz bandwidth). The maximum gain is obtained for both solutions at 64 GHz with G_{max} = 23.5 dB for the classical LWA and G_{max} = 19.7 dB for the GDSM-based LWA. This difference is simply explained by the fact that the simulated LWA is longer than the GDSM-based LWA.

V. Conclusion

A dispersion analysis is conducted to study different waveguide structures in order to design a LWA radiating in backward direction. A classical LWA is firstly designed using a GDS with metallic strip and is then compared to a more dispersive structure based on a metasurface with square patches. Simulations results are in good agreement with theoretical calculations and enhanced scanning capabilities are obtained with the metasurface. Indeed, a scanning range from -52° to -16° is achieved with the metasurface to be compared with a -28° to -14° range with a classical LWA using the same substrate and the same bandwidth of 11.6% at 60 GHz.

In future works, a wide bandwidth surface-wave launcher will be designed in order to fabricate and test the antenna in the 57 GHz-64 GHz frequency band.

Acknowledgment

This work was performed within the NOVIS60 project support by the CEFPRA (Indo-French Center for the Promotion of Advanced Research).

References

[1] T. Tamir and A. A. Oliner, “Guided complex waves. Part 1: Fields at an interface,” Proc. Inst. Electr. Eng., vol. 110, no. 2, pp. 310–324, Feb. 1963.

[2] M. Geiger, M. Hitzler, and C. Waldschmidt, “A flexible dielectric leaky-wave antenna at 160 GHz,” in 2017 47th European Microwave Conference (EuMC), 2017, pp. 240–243.

[3] M. K. Khattak and S. Kahng, “Enhanced gain metamaterial-based Leaky-wave beam-forming antenna for the V2X communication,” in 2015 International Conference on Emerging Technologies (ICET), 2015, pp. 1–2.

[4] S. K. Podilchak, A. P. Freundorfer, and Y. M. M. Antar, “Surface-Wave Launchers for Beam Steering and Application to Planar Leaky-Wave Antennas,” IEEE Trans. Antennas Propag., vol. 57, no. 2, pp. 355–363, Feb. 2009.

[5] B. Husain, M. Steeg, and A. Stöhr, “Estimating direction-of-arrival in a 5G hot-spot scenario using a 60 GHz leaky-wave antenna,” in 2017 IEEE International Conference on Microwaves, Antennas, Communications and Electronic Systems (COMCAS), 2017, pp. 1–4.

[6] H. Paaso et al., “DoA Estimation Using Compact CRLH Leaky-Wave Antennas: Novel Algorithms and Measured Performance,” IEEE Trans. Antennas Propag., vol. 65, no. 9, pp. 4836–4849, Sep. 2017.

[7] T. Zhang, J. Sarrazin, G. Valerio, and D. Istrate, “Estimation of Human Body Vital Signs Based on 60 GHz Doppler Radar Using a Bound-Constrained Optimization Algorithm,” Sensors, vol. 18, no. 7, Jul. 2018.

[8] H. Chuang, H. Kuo, F. Lin, T. Huang, C. Kuo, and Y. Ou, “60-GHz Millimeter-Wave Life Detection System (MLDS) for Noncontact Human Vital-Signal Monitoring,” IEEE Sens. J., vol. 12, no. 3, pp. 602–609, Mar. 2012.

[9] D. Comite et al., “A Dual-Layer Planar Leaky-Wave Antenna Designed for Linear Scanning Through Broadside,” IEEE Antennas Wirel. Propag. Lett., vol. 16, pp. 1106–1110, 2017.

[10] J. Liu, W. Zhou, and Y. Long, “A Simple Technique for Open-Stopband Suppression in Periodic Leaky-Wave Antennas Using Two Nonidentical Elements Per Unit Cell,” IEEE Trans. Antennas Propag., vol. 66, no. 6, pp. 2741–2751, Jun. 2018.

[11] M. H. Rahmani and D. Deslandes, “Backward to Forward Scanning Periodic Leaky-Wave Antenna With Wide Scanning Range,” IEEE Trans. Antennas Propag., vol. 65, no. 7, pp. 3326–3335, Jul. 2017.

[12] N. Nguyen-Trong, L. Zou, C. Fumeaux, and C. Caloz, “Ultra-high and Tunable Sensitivity Leaky-Wave Scanning Using Gain-Loss C-section Phasers,” ArXiv170606222 Phys., Jun. 2017.

[13] A. M. Patel and A. Grbic, “A Printed Leaky-Wave Antenna Based on a Sinusoidally-Modulated Reactance Surface,” IEEE Trans. Antennas Propag., vol. 59, no. 6, pp. 2087–2096, Jun. 2011.

[14] D. M. Pozar, Microwave Engineering, 4th Edition. Hoboken, NJ: John Wiley & Sons, 2011.

[15] O. Luukkonen et al., “Simple and Accurate Analytical Model of Planar Grids and High-Impedance Surfaces Comprising Metal Strips or Patches,” IEEE Trans. Antennas Propag., vol. 56, no. 6, pp. 1624–1632, Jun. 2008.

[16] J. Volakis, Antenna Engineering Handbook. McGraw-Hill Education, 2007.